ACERP: Vol. 5, No.1, (Winter 2019) 1-8

Advanced Ceramics Progress

Research Article

Journal Homepage: www.acerp.ir

Kinetics of photocatalytic degradation of methylene blue on nanostructured TiO2 coatings created by sol-gel process

M. Sajjadnejad[1,*], H. Karimi Abadeh[2]

[1] *Department of Materials Engineering, School of Engineering, Yasouj University, Yasouj, Iran*
[2] *Department of Materials Science and Engineering, School of Engineering, Shiraz University, Shiraz, Iran*

PAPER INFO

Paper history:

Received 22 January 2019
Accepted in revised form 29 July 2019

Keywords:

Rene-80
TiO2
Kinetics
methylene blue
photocatalyst
sol-gel process

ABSTRACT

Sol-gel process was chosen to produce a photocatalytic film to degrade methylene blue. In order to study structural and morphological properties of the coatings, a base sol of TTIP, I-PrOH, and DEA was prepared. Then with addition of 45g/L PEG 2000, 30g/L TiO2 and 15g/L PEG 2000 + 30g/L TiO2, to the base sol, three other sols were produced. The results of this study indicated that substrate can affect photocatalytic behavior of the coatings. Then different parameters (Sol types, number of dip coating cycles, initial concentration, two wavelengths of 265 and 254 nm and pH) of the study were modified and an equation was derived for each parameter. At last, using all the derived equations, a more general equation was calculated to predict the rate of corrosion based on pH, initial concentration of methylene blue, and number of dip coating cycles. A reactor was designed and tested to investigate the effect of continuous degradation. It was realized that the rate of all photocatalytic reactions were inhibited as a result of higher evaporation and decreased exposure time to coating and ultraviolet light.

1. INTRODUCTION

TiO_2 is used and studied extensively for its outstanding photocatalytic behavior [1-3]. Several additional unique properties such as non-toxicity, chemical stability in aqueous environments, and inexpensiveness make it a desirable semiconductor for industrial purposes. Due to inherent practical problems of using powder catalysts (i.e. homogenizing the powder throughout the whole medium and separation after treatment) for water treatment and purification processes, immobilized TiO_2 films have been extensively researched and utilized.

Diverse techniques like sputtering [4], electrospinning [2], chemical vapor deposition [5-7], and sol-gel process [8-14] can be used to produce the desired synthesis of TiO_2 film (or desired synthesized TiO_2 film). Among all these methods, sol-gel process has technical advantages due to its low cost, desirable homogeneity, and processing temperature. There are two feasible methods to produced TiO_2 films: the alkoxide route and the non-alkoxide route. Inorganic salts (such as $TiCl_4$) are used in alkoxide route as the starting material, then the inorganic anion will be removed which results in production of TiO_2. However, halides are notoriously challenging to remove and often remain in the material. On the other hand, TiO_2 films produced by this route are crystalline and possess high density [15].

Microstructure, density, and phase identity are key factors in shaping photocatalytic behavior of it. TiO_2 film produced by non-alkoxide route produces a network of material, so a calcination step should be carefully designed and undertaken to achieve the optimum photocatalytic properties, otherwise extensive deterioration of quality will occur.

Modified alkoxide sol-gel method has been extensively studied. The method was first studied by Balasubramanian et al. [15] in 2004. They established a more sensitive TiO_2 photocatalyst that could be produced by incorporating p-25 powder into an isopropoxide sol. Chen et al. [16, 17] found that the

* *Corresponding Author Email: M.sajjadnejad@yu.ac.ir; m.sajjadnejad@yahoo.com*

improvement in photocatalytic behavior was because of reduction in grain size, increase in number of pores, and presence of microcracks and crystalline material on the surface of the coating. Addition of polyethylene glycol (PEG) to alkoxide solution and its impact on increasing the thickness of TiO_2 film and morphology was first reported by Kato et al. [18]. These new findings help to reach to a well understanding of PEG effect on TiO_2 film produced by sol-gel method [19-22]. There are also some studies on the effect of crystal size and phase transformation during calcination steps [23, 24].

One of the main organic pollutants of many industries such as pharmaceutical, dyeing, printing, paper, and ink industries is an organic solution called methylene blue (Mb). Fortunately, this aqueous contamination can be removed easily using a photocatalysis method. There are several advantages in utilizing this route including cost-effectiveness, solar light energy source, and operation at near ambient temperatures.

The kinetics of anatase to rutile phase transformation and their effect on photocatalytic degradation have been studied by some researchers; however, to the best of our knowledge, the effect of parameters modifications on photocatalytic degradation of TiO_2 is not studied yet [25-28]. It is also noteworthy to mention that all of the reviewed) papers show a distinctive linear logarithmic curve [29-32].

In our previous work [33, 34], we extensively studied the effect of parameters modification on photocatalytic behavior of TiO_2 coating. The aim of this study was to synthesize a nanostructured TiO_2 film from a sol-gel containing both p-25 and PEG and then study the kinetics of degradation reactions on the surface of the resulted TiO_2 films. The beneficiality of parameters modifications was also investigated. Production of reactive film using sol-gel method was introduced in this work for the first time. Since most of the studies were performed under a stagnant system where the amount of material degradation was fixed, a reactor was designed to investigate the effect of Mb continuous degradation under an optimized condition.

2. MATERIALS AND METHODS

2.1. Materials and Chemicals

TiO_2 films were produced by the sol-gel method and then, their structural and morphological properties were studied. To get a clearer understanding of different affecting parameters, four different sols were prepared. Table 1 presents the materials that were used to create the sols. Methylene blue (Mb) was used to understand which TiO_2 film possessed superior photocatalytic behavior.

2.2. Preparation of TiO_2 Films by sol-gel Method

First, a base sol was prepared and then, three derivative sols were prepared based on it in order to investigate the effects of different sol additives. To prepare the base sol, TTIP, i-PrOH, and DEA were in terms of DEA:TTIP=4:1. Stirring was done for 2 hours and then deionized H_2O:TTIP at 2:1 molar ratio was added. To prepare the three other sols, 15g/L PEG 2000 (Sol 2), 30g/L TiO_2 (Sol 3) and 15g/L PEG 2000 + 30 g/L TiO_2 (Sol 4) were added to the base sol. Figure 1 shows the preparation steps of different sols schematically.

TABLE 1. Materials used to prepare sols

Material	Original company and purity (%)	Chemical formula and molar mass	Molecular structure
Titanium isopropoxide (TTIP)	Aldrich (97%)	$C_{12}H_{28}O_4Ti$ (284.215 g/mol)	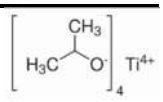
Isopropyl alcohol (i-PrOH)	Merck (99.99%)	C_3H_8O (60.10 g/mol)	
Diethylamine (DEA)	Aldrich (99%)	$C_4H_{11}N$ (73.14 g/mol)	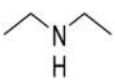
Polyethylene glycol (PEG)	Merck (99.9%)	$C_{2n}H_{4n+2}O_{n+1}$ (2000 g/mol)	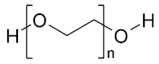

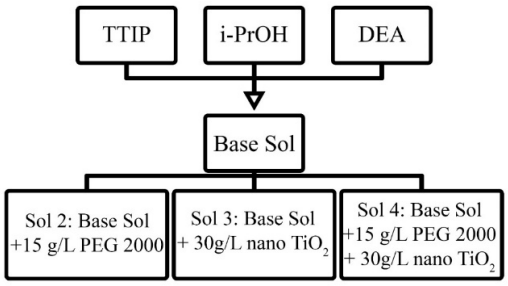

Figure 1. Schematics of sols preparations steps

Dip coating method was utilized to produce the TiO_2 films. A substrate of 304 stainless steel was used throughout the experiments. The withdrawal rate was chosen to be 13.5 $cm.min^{-1}$. In order to increase the films thickness, 1 to 6 dipping cycles were performed. After each dip-coating cycle, specimens were dried for 2 hours at 120 °C and subsequently each sample was calcined in an oven at 400 °C to 700 °C (calcination is necessary to obtain crystallized anatase phase). In order to minimize the nucleation of cracks in the coating surface, a slow heating rate of 3 $°C.min^{-1}$ was chosen. Since the literature showed that the logarithmic curve of Mb degradation is linear, all the tests were done in three points [29-32]. The mechanisms and production of the photocatalytic films are discussed in more detail in our previous studies [29, 30].

2.3. Degradation Reactor Design

A reactor was designed (Figure 2 & 3) to experiment the effect of continuous degradation of Mb. Two UV lamps with a wavelength of 254 nm and with the power of 8 W were utilized. The solutions were poured on the sloped coated surface to be exposed to UV light. Caution was taken to prevent evaporation.

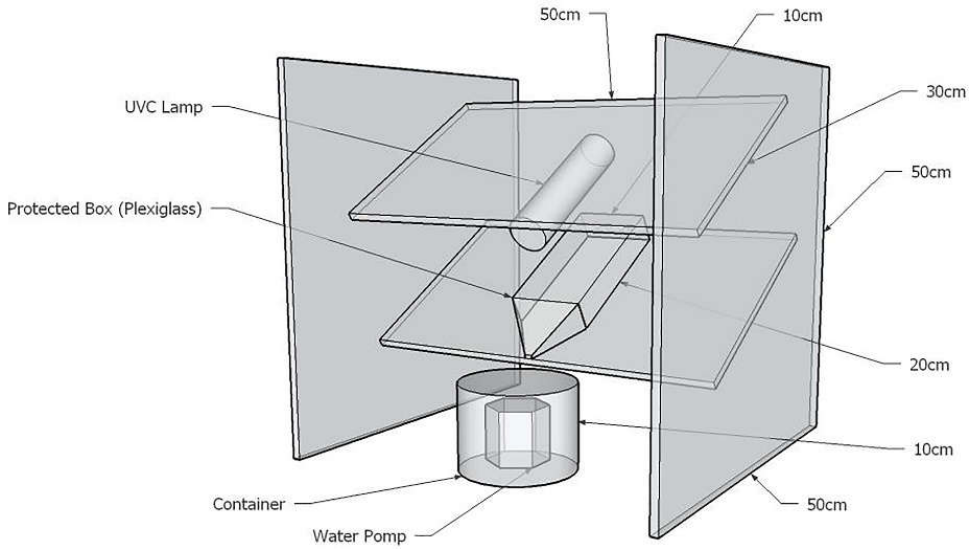

Figure 2. Schematics of the designed reactor

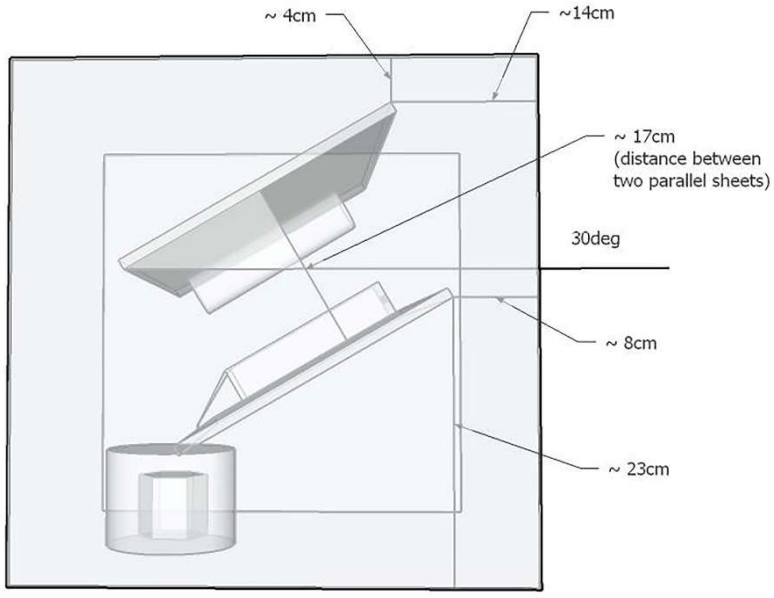

Figure 3. Side view schematics of the designed reactor.

3. RESULTS AND DISCUSSION

3.1. Crystallite Size

Crystallite size of achieved powders was calculated using Sherrer's equation:

$$D = \frac{0.89\,\lambda}{\beta \cos\theta} \quad (1)$$

Where D is the mean crystallite size, λ is the wavelength of X-ray used (related to the material used as the cathode). In this work, the machine used a Cu-K_α cathode with a wavelength of 1.54187 A°. Beta (β) is the

line broadening at half maximum intensity of peaks and θ is the Bragg's angle. The calculated results for the base sol and the forth sol (PEG+P25) are presented in Table 2. It can be seen that by elevating the temperature, the size of crystallites increased from 29.6 nm to 52.1 nm in the base sol. Same trend was seen for crystallite size of the forth sol, however, the biggest crystallite (24 nm) in this sample was still smaller than the lowest crystallite size in the base sol which is due to easier nucleation in the presence of P-25+PEG in the (forth) sol.

It should be noted that the errors of instruments were not taken into effect. Also, the crystals were assumed to be perfect with no trace of residual strain. Although Sherrer's equation possesses a ten percent error in the range of 0.5-10 μm crystallite size and higher percent errors for nano-crystallites, in the present study it can proved that this equation is appropriate for the prepared nano crystallites and comparison of their size with each other [35]. It is also worth mentioning that crystallinity affects degradation capabilities of a film to a high degree [36-38], so that it can have a synergetic effect with some environmental parameters [37]. To our understanding, higher crystallinity and open microstructures are generally considered to be superior photodegrading materials [36, 38].

TABLE 2. Crystallite size at different temperatures

Temperature (°C)	Crystallite size (nm), base sol	Crystallite size (nm), P-25+PEG
400	29.6	19
500	35.1	21.2
600	42.4	21.6
700	52.1	24.3

3.2. Calculation of Grain Size Based on SEM Pictures

As mentioned before, Sherrer's equation for crystallite under 500 nm possesses high error, so it was decided to do complementary analysis bases on SEM pictures. Figure 4 shows the created layer on 4 different prepared sols, baked at 500 °C.

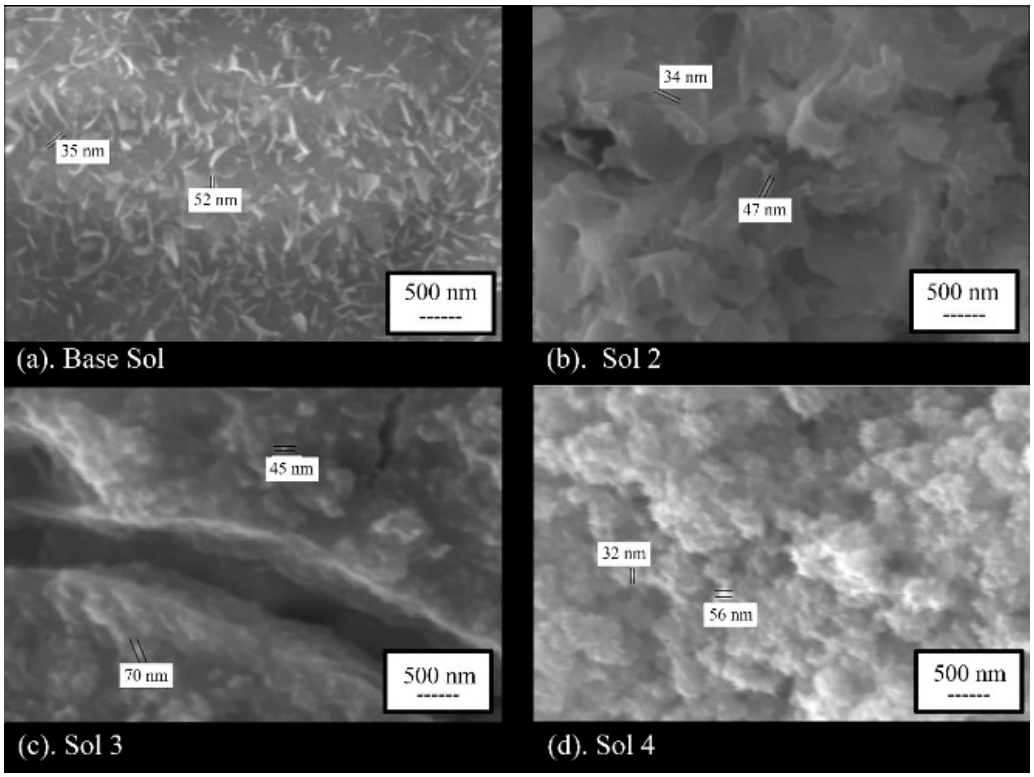

Figure 4. SEM micrograph(s) of coatings created in 4 different sols and their respective grain size

Mean grain size was calculated using Clemex™ Software. It can be observed that the crystallines size calculated in this method are larger than that in Table 2. Based on the SEM photomicrographs, the mean grain size of all samples were calculated to be 42nm; this might be the result of probable agglomeration that can happen during the coating process. Furthermore, both Clemex software and Sherrer's equation are susceptible to errors as mentioned previously.

3.3 Kinetics Studies

3.3.1. Effect of Different Sols on the Kinetics of Photocatalytic Reactions

Our previous study has established that addition of P-25 and PEG to the coating enhanced the photocatalytic behavior of coatings with the best performance seen for P-25+PEG (forth sol) coating. It is believed that addition of PEG and P-25 can increase the surface roughness of coating and thus, increase the available area for photocatalytic reactions. According to the Langmuir-Hinshelwood model, the slope of the plotted data is rqual to the reaction rate constant that are reported in Table 3. As expected, the fourth sol containing P-25+PEG had the highest rate constant and was the best photocatalytic coating in the present study.

TABLE 3. Effect of different sols on reaction rate constant

Sol type	The reaction rate constant, K (min^{-1})
Base sol	3.66×10^{-3}
PEG	3.69×10^{-3}
P-25	4.21×10^{-3}
PEG+P-25	1.02×10^{-2}

3.3.2. Effect of Number of Dip-coating Cycles on Kinetics of Photocatalytic Reaction

In order to investigate the effect of dip coating cycles on photocatalytic behavior, three different samples were prepared by coating the forth sol (P-25+PEG) for 1, 2 and 4 dip coating cycles. The concentration of Mb in solution was 5 ppm and an 8 W light with 254 nm wavelength was utilized. As presented in Table 4, effective catalytic behavior increased with increasing the number of dip coating cycles. As discussed in our previous work, increasing the number of deep coating cycles produced a rougher surface with higher amounts of reaction sites and thus, the photocatalytic behavior of TiO_2 was enhanced.

The rate of each photocatalytic reaction was calculated using the Langmuir-Hinshelwood model, and an increase of 4×10^{-3} min^{-1} was seen for each time dip coating cycle increases. It is possible to calculate the rate of reaction from the slope of the graph presented in Figure 5. A linear equation (2) was obtained where K is the reaction rate constant and N is the number of dip coating cycles. Other studies obtained a linear logarithmic curve of Mb degradation using only three reference points [29-32].

$$Ln(K) = 1.117\ Ln(N) - 5.553 \quad (2)$$

TABLE 4. Effect of number of dip-coating cycles on reaction rate constant

Number of Dip-coating cycles	Percentage of decomposition	The reaction rate constant, K (min^{-1})
1	30%	3.90×10^{-3}
2	66%	8.25×10^{-3}
4	77%	1.84×10^{-2}

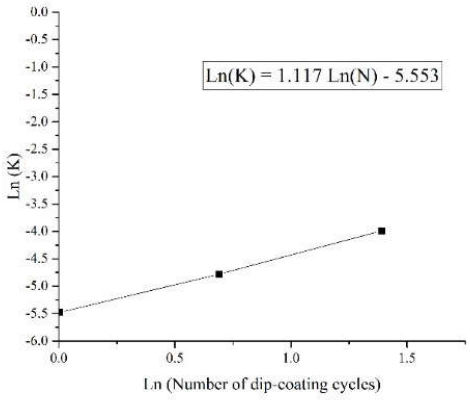

Figure 5. Dependence of Linear graph of reaction rate on the number of dip -coating cycles

3.3.3. Effect of Initial Concentration of Mb on Kinetics of Photocatalytic Reaction

Effect of the initial concentration of Mb was investigated on a fourtimes dip cycles of P-25+PEG sol coating sample. The initial concentrations of Mb were 2, 5, and 10 ppm and a light source of 160 W with a wavelength of 365 nm was used. The results of photodegradation after 120 minutes of exposure are presented in Table 5. It was observed that the photodegradation of Mb decreased with increasing its initial concentration. Several other studies reported the same behavior for photodegradation of organic compounds and dyes [39, 40]. It was theorized that when the initial concentration of a dye increases in the solution, the amount of absorbed Mb molecules on the surface of TiO_2 increases; thus, limiting the direct interaction of other molecules with generated holes and hydroxyl radicals. The other reason is that the higher amount of Mb molecules in bulk solution can absorb more amount of UV light and lessen the number of photons that reach the surface of TiO_2 film. This, in turn, decreases the hydroxyl radical flux [41] that ultimately results in a lower amount of Mb degradation at higher initial concentrations.

TABLE 5. Effect of initial concentration on reaction rate constant

The initial concentration of Mb (ppm)	Percent of degradation (%)	The reaction rate constant, K (min^{-1})
2	52	1.44×10^{-2}
5	52	1.11×10^{-2}
10	35	5.40×10^{-3}

The graph of Ln(K)/ Ln (Initial concentration) (Figure 6) was plotted based on Langmuir-Hinshelwood model and the equation of effect of initial concentration (Equation 3) was calculated based on this plot.

$$Ln(K) = -0.5924Ln(C0) \quad (3)$$

3.3.4. Effect of Wavelength

Two UV wavelength and three initial concentrations of Mb were used to investigate the effect of UV wavelength on the degradation of Mb. The coatings were prepared of P-25+PEG (forth sol) and made by four times of dip-coating. Based on the results presented in Table 6, it can be seen that the lamp with 254 nm wavelength degraded more Mb than the lamp with 365 nm wavelength. [33], The energy of light is a more important factor in its degradating ability rather than its power, so a less powerful lamp with higher energy light can degrade more amount of Mb compared to a more powerful lamp with a longer wavelength light. Also, it was found that 254 nm lights are the worst case scenario when it comes to Mb degradation and other studies found out that solar light is more beneficial in this regard [29-32], so using a 254 nm lamp gives us a baseline for technical purposes.

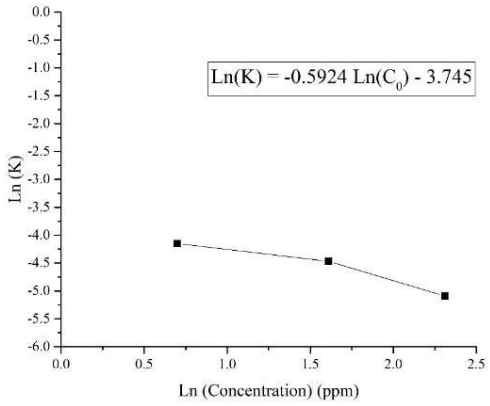

Figure 6. Linear graph of reaction rate dependence on the initial concentration of Mb

It was reported that for a coating that is calcined at 500 °C, the optimum absorption happens at around 250 nm and drops significantly around 400 nm.

3.3.5. The Effect of pH

The effect of pH on coating photocatalytic performance was investigated in the pH range of 3-9. It was reported that the rate of degradation increased with increasing pH. Reaction rate constants (K) were calculated using $Ln(C_0/C)$ by time and reported in Table 7. Figure 8 shows the fluctuation of Ln(K) by Ln(pH) and Equation 6, derived from the Figure 7, shows the relation between the rate of reaction and pH.

$$Ln(K) = 0.7702\ Ln(pH) - 4.967 \quad (6)$$

By taking into account the initial and final concentration of the system and implementing this data in Ln(K) – $Ln(C_0)$, a linear relation was obtained that is plotted in Figure 7. Equations 4 and 5 are the calculated equations for 365 nm and 254 nm wavelengths, respectively.

$$Ln(k) = -0.5924\ Ln(C_0) - 3.745 \quad (4)$$

$$Ln(k) = -0.524\ Ln(C_0) - 3.294 \quad (5)$$

TABLE 6. Effect of wavelength on reaction rate constant

Initial Concentration (ppm)	Degradation with 365 nm wavelength (%)	Degradation with 254 nm wavelength (%)	The reaction rate constant for 365 nm wavelength, K (min^{-1})	The reaction rate constant for 254 nm wavelength, K (min^{-1})
10	35	66	5.40×10^{-3}	1.15×10^{-2}
5	52	78	1.11×10^{-2}	1.50×10^{-2}
2	51	94	1.44×10^{-2}	2.65×10^{-2}

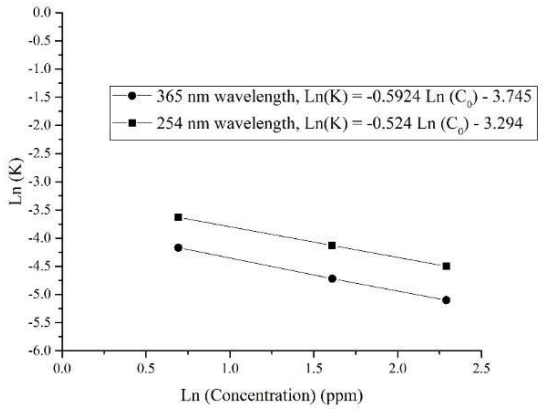

Figure 7. Dependency of reaction rate (slope of the linear graph) on wavelength

TABLE 7. Effect of pH on reaction rate constant

pH of the Sol	Reaction rate constant, K (min^{-1})
3	1.65×10^{-3}
6	2.65×10^{-2}
9	3.89×10^{-2}

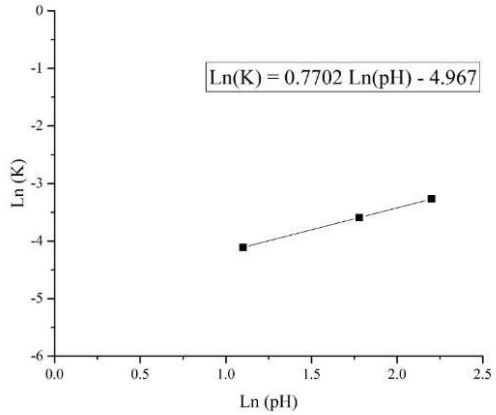

Figure 8. Dependency of linear graph of reaction rate on pH

3.3.6. Overview of Parameters Modifications

Figure 9 shows the effects of parameters modifications on the whole process. At the first step, effect of different sols was analyzed and the best sol was chosen. Then, the effects of number of dip coating, initial concentration, and pH were analyzed progressively and the best environment for the best result was obtained. It can be clearly observed that the rate of decomposition reaction was increased 10 times from the lowest of 3.66×10^{-3} min^{-1} to 3.89×10^{-2} min^{-1}. This finding can prove the effectiveness of this research and also our previously studies [33, 34].

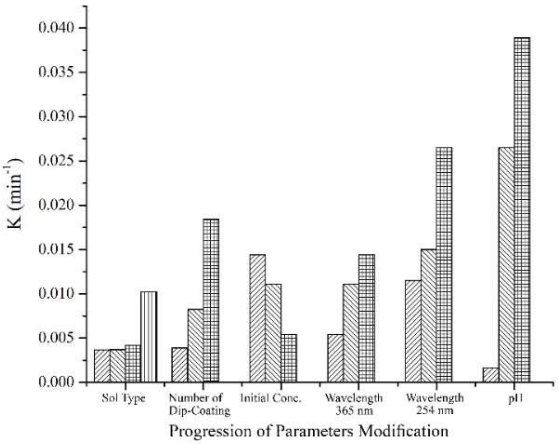

Figure 9. Progression of modifications done to experimental parameters

A general equation can be derived based on the Equations 2 to 6 (equations are based on K) :

$$Ln(K) = 1.117\ Ln(N) - 5.553 \rightarrow K = \mathbf{k}_1 N^{1.117} \quad (7)$$

(N: the number of dip coating cycle)

$$Ln(k) = -0.5924 Ln(C_0) - 3.745 \rightarrow K = \mathbf{k}_2 C_0^{-0.5924} \quad (8)$$

(C_0: initial concentration)

$$Ln(K) = 0.7702 Ln(pH) - 4.967 \rightarrow K = \mathbf{k}_3 pH^{0.7702} \quad (9)$$

By multiplying these equations, we get to the general equation where $\mathbf{k}_0 = \mathbf{k}_1 \times \mathbf{k}_2 \times \mathbf{k}_3$, which is dependent on N, C_0 and pH.

$$K = \mathbf{k}_0 C^{-0.592} (pH)^{0.77} N^{1.117} \quad (10)$$

3.4. Continuous Degrading Setup

Using the contentious degrading setup, it was found that this setup did not perform on par with our experimental setup and decreased the reaction rate up to 10% of the highest rate. It was seen that the velocity of the solution layer was higher than needed and as a result, the amount of exposure time was reduced and the degradation decreased. The other point is that the amount of evaporation was higher in this setup (continuous method) compared to stationary experiments.

4. CONCLUSION

Sol-gel process was chosen to produce a photocatalytic film to degrade methylene blue. Kinetic of reactions were investigated and a general equation was derived based on the initial concentration of methylene blue, the number of dip-coating cycles, and pH.. Contentious degradation of Mb showed that due to the higher evaporation and lower exposure time, the rate of all reactions were slowed down.

REFERENCES

1. Sreethawong, T., Ngamsinlapasathian, S., Yoshikawa, S., "Surfactant-aided sol–gel synthesis of mesoporous-assembled TiO_2–NiO mixed oxide nanocrystals and their photocatalytic azo dye degradation activity", ***Chemical engineering journal***, Vol. 192, (2012), 292-300.
2. Li, D., Pan, C., "Fabrication and characterization of electrospun TiO_2/CuS micro–nano-scaled composite fibers", ***Progress in Natural Science: Materials International***, Vol. 22, No. 1, (2012), 59-63.
3. Zhang, Y. P., Xu, J. J., Sun, Z. H., Li, C. Z., Pan, C. X., "Preparation of graphene and TiO_2 layer by layer composite with highly photocatalytic efficiency", ***Progress in Natural Science: Materials International***, Vol. 21, No. 6, (2011), 467-471.
4. Lai, C.W., Sreekantan, S., San E, P., Krengvirat, W., "Preparation and photoelectrochemical characterization of WO_3-loaded TiO_2 nanotube arrays via radio frequency sputtering", ***Electrochimica Acta***, Vol. 77, (2012), 128-136.
5. Mathur, S., Kuhn, P., "CVD of titanium oxide coatings: Comparative evaluation of thermal and plasma assisted processes", ***Surface and Coatings Technology***, Vol. 201, No. 3-4, (2006), 807-814.
6. Bessergenev, V. G., Mateus, M. D. C., Vasconcelos, D. A., Mariano, J. F. M. L., Botelho do Rego, A. M., Lange, R., Burkel, E., "TiO_2:(Fe, S) thin films prepared from complex precursors by CVD, physical chemical properties, and photocatalysis", ***International Journal of Photoenergy***, Vol. 2012, (2012).
7. Ma, L., Chen, A., Zhang, Z., Lu, J., He, H., Li, C., "In-situ fabrication of CNT/TiO_2 interpenetrating network film on nickel substrate by chemical vapour deposition and application in photoassisted water electrolysis", ***Catalysis Communications***, Vol. 21, (2012), 27-31.
8. Tseng, T. K., Lin, Y. S., Chen, Y. J., Chu, H., "A review of photocatalysts prepared by sol-gel method for VOCs removal", ***International journal of molecular sciences***, Vol. 11, No. 6, (2010), 2336-2361.
9. Macwan, D. P., Dave, P. N., Chaturvedi, S., "A review on nano-TiO_2 sol–gel type syntheses and its applications", ***Journal of materials science***, Vol. 46, No. 11, (2011), 3669-3686.
10. Hartmann, P., Lee, D. K., Smarsly, B. M., Janek, J., "Mesoporous TiO_2: comparison of classical sol− gel and nanoparticle based photoelectrodes for the water splitting reaction", ***Acs Nano***, Vol. 4, No. 6, (2010), 3147-3154.
11. El-Nahass, M. M., Ali, M. H., El-Denglawey, A., "Structural and optical properties of nano-spin coated sol–gel porous TiO_2

films", ***Transactions of Nonferrous Metals Society of China,*** Vol. 22, No. 12, (2012), 3003-3011.
12. Zhang, T., Oyama, T., Horikoshi, S., Zhao, J., Hidaka, H., Serpone, N., "Assessment and influence of operational parameters on the TiO_2 photocatalytic degradation of sodium benzene sulfonate under highly concentrated solar light illumination", ***Solar Energy,*** Vol. 71, No. 5, (2001), 305-313.
13. Liang, Y., Wang, H. S., Casalongue, H. S., Chen, Z., Dai, H., "TiO_2 nanocrystals grown on graphene as advanced photocatalytic hybrid materials", ***Nano Research,*** Vol. 3, No. 10, (2010), 701-705.
14. Alzamani, M., Shokuhfar, A., Eghdam, E., Mastali, S., "Influence of catalyst on structural and morphological properties of TiO_2 nanostructured films prepared by sol–gel on glass", ***Progress in Natural Science: Materials International,*** Vol. 23, No. 1, (2013), 77-84.
15. Balasubramanian, G., Dionysiou, D. D., Suidan, M. T., Subramanian, V., Baudin, I., Laîné, J. M., "Titania powder modified sol-gel process for photocatalytic applications", ***Journal of materials science,*** Vol. 38, No. 4, (2003), 823-831.
16. Chen, Y., Dionysiou, D. D., "A comparative study on physicochemical properties and photocatalytic behavior of macroporous TiO_2-P25 composite films and macroporous TiO_2 films coated on stainless steel substrate", ***Applied Catalysis A: General,*** Vol. 317, No. 1, (2007), 129-137.
17. Chen, Y., Dionysiou, D. D., "Bimodal mesoporous TiO_2–P25 composite thick films with high photocatalytic activity and improved structural integrity", ***Applied Catalysis B: Environmental,*** Vol. 80, No. 1-2, (2008), 147-155.
18. Kato, K., Tsuzuki, A., Torii, Y., Taoda, H., Kato, T., Butsugan, Y., "Morphology of thin anatase coatings prepared from alkoxide solutions containing organic polymer, affecting the photocatalytic decomposition of aqueous acetic acid", ***Journal of materials science,*** Vol. 30, No. 3, (1995), 837-841.
19. Su, Z., Zhang, L., Jiang, F., Hong, M., "Formation of crystalline TiO_2 by anodic oxidation of titanium", ***Progress in Natural Science: Materials International,*** Vol. 23, No. 3, (2013), 294-301.
20. Huang, W., Lei, M., Huang, H., Chen, J., Chen, H., "Effect of polyethylene glycol on hydrophilic TiO_2 films: Porosity-driven superhydrophilicity", ***Surface and Coatings Technology,*** Vol. 204, No. 24, (2010), 3954-3961.
21. Fan, S. Q., Li, C. J., Li, C. X., Liu, G. J., Yang, G. J., Zhang, L. Z., "Preliminary study of performance of dye-sensitized solar cell of nano-TiO_2 coating deposited by vacuum cold spraying", ***Materials transactions,*** Vol. 47, No. 7, (2006), 1703-1709.
22. Bu, S., Jin, Z., Liu, X., Yang, L., Cheng, Z., "Fabrication of TiO_2 porous thin films using peg templates and chemistry of the process", ***Materials Chemistry and Physics,*** Vol. 88, No. 2-3, (2004), 273-279.
23. Yu, J., Jimmy, C. Y., Ho, W., Jiang, Z., "Effects of calcination temperature on the photocatalytic activity and photo-induced super-hydrophilicity of mesoporous TiO_2 thin films", ***New Journal of Chemistry,*** Vol. 26, No. 5, (2002), 607-613.
24. Yu, J. G., Yu, H. G., Cheng, B., Zhao, X. J., Yu, J. C., Ho, W. K., "The effect of calcination temperature on the surface microstructure and photocatalytic activity of TiO_2 thin films prepared by liquid phase deposition", ***The Journal of Physical Chemistry B,*** Vol. 107, No. 50, (2003), 13871-13879.
25. Dariani, R. S., Esmaeili, A., Mortezaali, A., Dehghanpour, S., "Photocatalytic reaction and degradation of methylene blue on TiO_2 nano-sized particles", ***Optik,*** Vol. 127, No. 18, (2016), 7143-7154.
26. Shakibania, R., "Kinetic Model for Nanocrystalline Anatase to Rutile Polymorphic Transformation", ***Chemical and biochemical engineering quarterly,*** Vol. 31, No. 3, (2017), 353-359.
27. Ba-Abbad, M. M., Kadhum, A. A. H., Mohamad, A. B, Takriff, M. S., Sopian, K., Al-Shamali, S. S., "Kinetics transformation of anatase to rutile phase for titanium dioxide nanoparticles prepared by sol-gel method", ***Materials Science Forum***, Vol. 756, (2013), 11-15. Trans Tech Publications.
28. Hanaor, D. A., Sorrell, C. C., "Review of the anatase to rutile phase transformation", ***Journal of Materials science,*** Vol. 46, No. 4, (2011), 855-874.
29. Kuo, W. S., Ho, P. H., "Solar photocatalytic decolorization of methylene blue in water", ***Chemosphere,*** Vol. 45, No. 1, (2001), 77-83.
30. Lakshmi, S., Renganathan, R., Fujita, S., "Study on TiO_2-mediated photocatalytic degradation of methylene blue", ***Journal of Photochemistry and Photobiology A: Chemistry,*** Vol. 88, No. 2-3, (1995), 163-167.
31. Houas, A., Lachheb, H., Ksibi, M., Elaloui, E., Guillard, C., Herrmann, J. M., "Photocatalytic degradation pathway of methylene blue in water", ***Applied Catalysis B: Environmental,*** Vol. 31, No. 2, (2001), 145-157.
32. Lachheb, H. Puzenat, E., Houas, A., Ksibi, M., Elaloui, E., Guillard, C., Herrmann, J. M., "Photocatalytic degradation of various types of dyes (Alizarin S, Crocein Orange G, Methyl Red, Congo Red, Methylene Blue) in water by UV-irradiated titania", ***Applied Catalysis B: Environmental,*** Vol. 39, No. 1, (2002), 75-90.
33. Sohrabi, H., Mozafari, A., Sajjadnejad, M., Tabaian, S. H., Omidvar, H., "Influence of operational parameters on the TiO_2 photocatalytic degradation of Methylene blue", ***Materials Science and Technology,*** Vol. 32, No. 12, (2016), 1282-1288.
34. Sohrabi, H., Tabaian, S. H., Omidvar, H., Sajjadnejad, M., Mozafari, A., "Synthesis of nanostructured TiO_2 coatings by Sol-Gel method: structural and morphological studies", ***Synthesis and Reactivity in Inorganic, Metal-Organic, and Nano-Metal Chemistry,*** Vol. 46, No. 3, (2016), 414-422.
35. Azároff, L. V., Donahue, R. J., "Laboratory experiments in x-ray crystallography", McGraw-Hill New York, (1969).
36. Eufinger, K., Poelman, D., Poelman, H., De Gryse, R., Marin, G. B., "Effect of microstructure and crystallinity on the photocatalytic activity of TiO_2 thin films deposited by dc magnetron sputtering", ***Journal of Physics D: Applied Physics,*** Vol. 40, No. 17, (2007), 5232.
37. Cong, S., Xu, Y., "Explaining the high photocatalytic activity of a mixed phase TiO_2: a combined effect of O_2 and crystallinity", ***The Journal of Physical Chemistry C,*** Vol. 115, No. 43, (2011), 21161-21168.
38. Yu, J. C., Yu, J., Ho, W., Jiang, Z., Zhang, L., "Effects of F-doping on the photocatalytic activity and microstructures of nanocrystalline TiO_2 powders", ***Chemistry of materials,*** Vol. 14, No. 9, (2002), 3808-3816.
39. Elfanaoui, A., Elhamri, E., Boulkaddat, L., Ihlal, A., Bouabid, K., Laanab, L., Taleb, A., Portier, X., "Optical and structural properties of TiO_2 thin films prepared by sol–gel spin coating", ***International Journal of Hydrogen Energy,*** Vol. 36, No. 6, (2011), 4130-4133.
40. Brinker, C. J., Hurd, A. J., Schunk, P. R., Frye, G. C., Ashley, C. S., "Review of sol-gel thin film formation", ***Journal of Non-Crystalline Solids***, Vol. 147, (1992), 424-436.
41. Schubert, D. W., Dunkel, T., "Spin coating from a molecular point of view: its concentration regimes, influence of molar mass and distribution", ***Materials Research Innovations,*** Vol. 7, No. 5, (2003), 314-321.